Effects of a vertical wall on wave power absorptions with wave energy converters arrays

KARA, Fuat

Renewable Energy 196 (2022) 812–823

Contents lists available at ScienceDirect

Renewable Energy

journal homepage: www.elsevier.com/locate/renene

Effects of a vertical wall on wave power absorption with wave energy converters arrays

Fuat Kara

Sheffield Hallam University, Howard Street, Sheffield, S1 1WB, UK

ARTICLE INFO

Article history:
Received 15 October 2021
Received in revised form
6 July 2022
Accepted 8 July 2022
Available online 14 July 2022

Keywords:
Wave power absorption
Mean and individual interaction factors
Multibody interaction in front of a vertical wall
Transient wave green function
Boundary integral equation
Method of images

ABSTRACT

The application of in-house transient wave-body interaction ITU-WAVE computational tool is extended to predict the wave power absorption with Wave Energy Converters (WECs) arrays in front of a vertical wall using time dependent boundary integral equation method. The vertical wall effect is taken into account with method of images which considers the perfect reflection of incident waves from a vertical wall. The effects of separation distance between WECs as well as a vertical wall and WECs, and heading angles are studied to predict wave power absorption, mean and individual interaction factors which determine the performances of WECs arrays. The numerical results of WECs arrays in front of vertical wall show that both radiation and exciting force parameters are quite different from those of without a vertical wall. The numerical investigations also demonstrate that wave power absorption with an array system in front of a vertical wall are significantly greater than those of without a vertical wall. This is due to nearly trapped and standing waves between a vertical wall and WECs. The prediction of hydrodynamic parameters in front of a vertical wall with present ITU-WAVE are validated against other published numerical, analytical, and experimental results which show satisfactory agreements.

1. Introduction

The efficiency of the wave power absorption from ocean waves with isolated Wave Energy Converters (WECs) without or with control strategies [1] can be increased by changing and modifying the geometry, wave heading angles, absorption modes with single and multimode, Power-Take-Off (PTO). However, if the significant amount of electricity generation is required, the array arrangements of WECs need to be exploited in either offshore environment with higher energy contents or near shore. The absorption performances of WECs depend also on draft and separation distances between WECs in an array system [2].

The maintenances, operations and installations increase overall costs considerably in the offshore environment although available wave power is higher. In this case, the cost reduction can be achieved by integrations of the isolated or WECs arrays with other near-shore coastal structures (e.g., breakwaters) or deployments of WECs in front of a vertical wall. In addition to the cost reductions, the integration of WECs with other coastal structures increases the wave power absorptions due to the hydrodynamic interactions of the reflected waves with WECs which are placed in front of the vertical coastal structures [3–5]. There are many studies and investigations related to deployment of WECs arrays in front of marine structures [5–7] including stationary [3], flexible [9] and floating [10] breakwater. The integrated WECs arrays with stationary, flexible and floating breakwater include Oscillating Water Column (OWC), overtopping, piston type, oscillating buoys, pile-strained floating breakwater, embedded OWC chamber [11–14].

The flow behaviour around WECs arrays in front of a vertical wall can be predicted with method of images for the prediction of radiation and exciting force Impulse Response Functions (IRFs). Method of images uses the WECs arrays in front of a vertical wall and their images considering a vertical wall as a reference line. This method is applied for the prediction of frequency domain hydrodynamic coefficients and exciting forces of single WEC or arrays in a channel [15] as well as the deployment of an isolated WEC or arrays in front of a vertical breakwater [16,17]. A vertical breakwater can be considered either infinite length wall considering the perfect reflection of waves from vertical wall [18] with method of images or finite length wall [16] considering the effects of finite length of a vertical wall on the predictions of the hydrodynamic parameters. Wave power absorption in front of a vertical wall requires the prediction of the radiation and exciting forces using analytical or

E-mail address: fuat.kara@shu.ac.uk.

https://doi.org/10.1016/j.renene.2022.07.046

numerical frequency domain methods with two [19] and three-dimensional analyses [8,20] or time domain methods with transient wave Green function [5] as studied and presented in the present paper.

The solutions of the hydrodynamic radiation and exciting forces to predict the hydrodynamic performance of WECs in front of a vertical wall can be approximated with three commonly used methods. These methods include the analytical and numerical frequency as well as time domain methods. The most used numerical frequency and time domain methods in three-dimensional analyses are Boundary Integral Equation Methods (BIEM) using frequency and transient wave Green functions [2,5,21–24] and Rankine type Green function [25,26]. If the WECs geometries are defined analytically, the analytical methods including point absorber [27], plane wave analysis [28] and direct matrix method [29] can then be used to predict the performance of WECs arrays.

Although the hydrodynamic performances and wave power absorptions with WECs arrays are studied extensively in the literature, the limited numbers of papers exist to exploit the novelty of the wave power absorption with WECs in front of a vertical wall. The exploitation of a vertical wall increases the efficiency of WECs arrays due to strong hydrodynamic interactions between a vertical wall and WECs arrays. In addition, most of the existence literatures is mainly focused on the exciting force predictions without giving much attention to the radiation force calculations. The present paper aims to contribute and fill these knowledge gap in the literature. Furthermore, to the best of author's knowledge, the numerical analysis of radiation and exciting forces with direct time domain methods using three-dimensional transient wave Green function for the predictions of wave power absorption with WECs arrays in front of a vertical wall are not studied before in the literature in the context of the potential theory and linear formulation. This is another contribution to knowledge and novel part of the present study.

2. Equation of motion of multibody interaction of array systems

The linearized initial-boundary value problem in time domain is predicted with body-fixed Cartesian coordinate system $\vec{x} = (x, y, z)$ in Fig. 1 which describes the fluid flow around WECs in an array system. The centre of xy-plane, which is on $z = 0$, is selected as the origin of the body-fixed coordinate system. The positive direction of z-axis is upwards and that of x-axis is towards the forward. The fluid boundaries are defined by surface at infinity S_∞, WEC surface $S_b(t)$, intersection between WEC and free surface Γ, and free surface $S_f(t)$ in Fig. 1 [22].

In Fig. 1, d represents the separation distance between WECs in an array system whilst wl is used for the separation distance between WECs arrays and a vertical wall. β is for heading angle (e.g., $\beta = 90^\circ$ is for beam seas). Numbers (1,2,3,4,5) are the positions of WECs in an array system. The behaviour of floating WECs arrays is represented with equation of motion in time domain [30] in Eq. (1).

$$\sum_{k=1}^{6}\left(M_{kk}^{i}+a_{kk}^{i}\right)\ddot{x}_{k}^{i}(t)+\left(b_{kk}^{i}+B_{PTO_{kk}}^{i}\right)\dot{x}_{k}^{i}(t)+\left(C_{kk}^{i}+c_{kk}^{i}\right)x_{k}^{i}(t)+\int_{0}^{t}d\tau K_{kk}^{i}(t-\tau)\dot{x}_{k}^{i}(\tau)=\int_{-\infty}^{\infty}d\tau K_{kE}^{i}(t-\tau)\zeta(\tau) \tag{1}$$

where the rigid body modes of surge, sway, heave, roll, pitch, and yaw are given with $k = 1, 2, 3, \ldots, 6$ respectively whilst the number of WECs, N, in an array system is presented with $i = 1, 2, 3, \ldots, N$. The displacements, velocities, and accelerations of each WEC at their mean positions are given by $x_k^i(t) = (1, 2, 3, \ldots, N)^T$, $\dot{x}_k^i(t)$ and $\ddot{x}_k^i(t)$ respectively at which dot represents the time derivatives. The inertia mass matrix and hydrostatic restoring coefficients matrix in Eq. (1) are given with M_{kk}^i and C_{kk}^i respectively [2,5]. The instantaneous forces due to oscillations of WECs arrays are given with a_{kk}^i, b_{kk}^i and c_{kk}^i coefficients which are proportional to acceleration, velocity, and displacement of WECs respectively. The free-surface effect due to oscillations of WECs in an array system is given by radiation IRFs $K_{kk}^i(t)$ [31] which is obtained by time marching of boundary integral equations for each WEC at each time step [22,32,37–39]. The time dependent exciting forces and moments due to arbitrary uni-directional impulsive incident wave elevation $\zeta(t)$ are given on the right-hand side of Eq. (1) [32]. As maximum wave power is absorbed at the resonant frequency [33], the diagonal elements of damping coefficients of PTO matrix $B_{PTO_{kk}}^i$ are considered as the wave damping coefficient of an isolated WEC at resonant frequency in Eq. (1). The equation of motion Eq. (1) is then solved with fourth-order Runge-Kutta method [1,2,5,22–24,34–36].

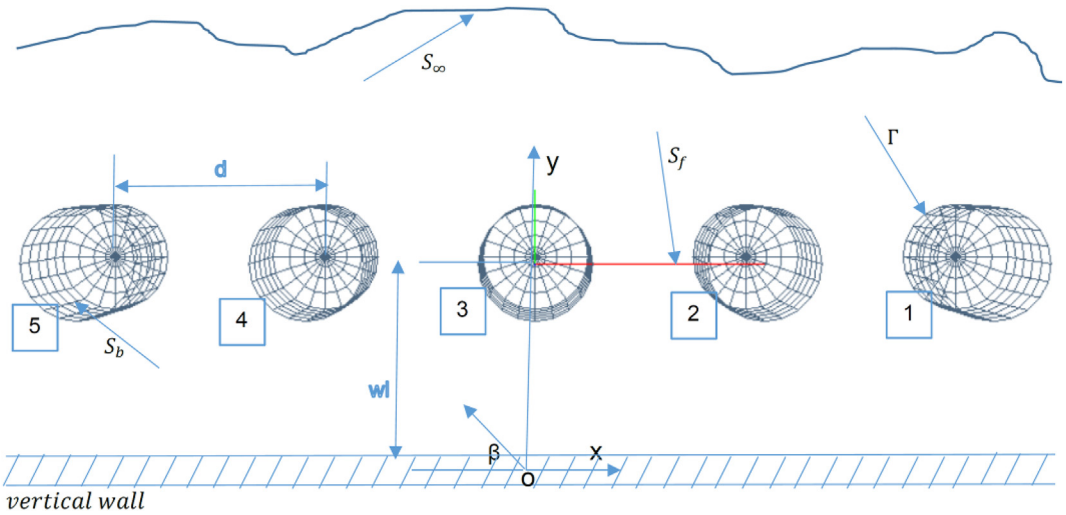

Fig. 1. Coordinate system and surface of WECs in a linear 1 × 5 array system.

3. Instantaneous wave power, individual and mean interaction factors

PTO is used to absorb the instantaneous wave power, $P^i_{ins_k}(t)$, at each mode with WECs in an array system. $P^i_{ins_k}(t)$ is the functions of the radiation and exciting forces and is given with Eq. (2).

$$P^i_{ins_k}(t) = \left[F^i_{exc_k}(t) + F^i_{rad_k}(t)\right] \cdot \dot{x}^i_k(t) \tag{2}$$

where $F^i_{exc_k}(t)$ is the exciting forces whilst $F^i_{rad_k}(t)$ is the radiation forces [1,2]. $\dot{x}^i_k(t)$ is the velocity of each WEC in array system. The time dependent mean wave power, $\overline{P}^i_{ins_k}(t)$, in Eq. (3), which is absorbed by PTO system over a time range T, may be written as

$$\overline{P}^i_{ins_k}(t) = \frac{1}{T}\int_0^T dt \cdot \left[F^i_{exc_k}(t) + F^i_{rad_k}(t)\right] \cdot \dot{x}^i_k(t) \tag{3}$$

The mean absorbed wave power in Eq. (3) and other time dependent parameters are predicted considering only the last half of the time domain simulation results to avoid the transient effects.

$$\overline{P}_{T_k}(t) = \sum_{i=1}^{N} \overline{P}^i_{ins_k}(t) \tag{4}$$

The total mean absorbed wave power, $\overline{P}_{T_k}(t)$, for N numbers of arrays and for mode k is presented in Eq. (4). The individual interaction factor, $q^i_{ind_{v_k}}(\omega)$, and mean interaction factor $q_{mean_k}(\omega)$ at any incident wave frequency, ω, is given [40].

$$q^i_{ind_{v_k}}(\omega) = \frac{\overline{P}^i_{ins_k}(\omega)}{\overline{P}^0_{ins_k}(\omega_n)}\ ,\ q_{mean_k}(\omega) = \frac{\overline{P}_{T_k}(\omega)}{N \times \overline{P}^0_{ins_k}(\omega_n)} \tag{5}$$

where $\overline{P}^0_{ins_k}(\omega_n)$ is the absorbed wave power with an isolated WEC at resonant frequency. $\overline{P}^i_{ins_k}(\omega)$ at the incident wave frequency, ω, is the mean value of $\overline{P}^i_{ins_k}(t)$ in Eq. (3) whilst $\overline{P}^0_{ins_k}(\omega_n)$ at the natural frequency, ω_n, is the mean value of $\overline{P}^0_{ins_k}(t)$. $\overline{P}_{T_k}(\omega)$ represents the total absorbed wave power with N number of WECs in mode k (e.g., heave). $\overline{P}_{T_k}(\omega)$ at the incident wave frequency, ω, is the mean value of $\overline{P}_{T_k}(t)$ in Eq. (4).

4. Numerical results and discussions

4.1. Validation of in-house transient wave-multibody ITU-WAVE numerical results

4.1.1. Validation of radiation force coefficients

Before the presentation of the power absorption from ocean waves with WECs arrays with and without a vertical wall effect, ITU-WAVE computational results are compared with other published numerical, analytical, and experimental results for the validation purposes. Truncated vertical cylinder of linear 1 × 5 arrays with radius R, draft T = R, separation distance between WECs d = 8R, and separation distance between a vertical wall and WECs arrays wl = 4R is used for the prediction of present ITU-WAVE numerical results which are approximated with method of images and compared with analytical results of [18]. The computed numerical results at panel number 256 on single WEC, total 1280 panel for linear 1 × 5 arrays in Fig. 1, is converged and used for the present ITU-WAVE numerical calculations with non-dimensional time step size, $t\sqrt{g/R} = 0.05$. ITU-WAVE radiation diagonal IRF of WEC1 ($K^{11}_{22}(t)$) in sway mode is presented in Fig. 2(a) whilst the interaction IRF in sway mode between WEC1 and WEC3 ($K^{13}_{22}(t)$) are presented in Fig. 2(b). In $K^{13}_{22}(t)$, the subscript represents the mode of motion (e.g., 22 is used for sway-sway mode) whilst the superscript represents WECs numbers in an array system (e.g., 13 is used for the interaction of WEC1 and WEC3). When the sway interaction IRF are compared with diagonal IRF, it can be observed from Fig. 2(a) and (b) that the behaviour of interaction IRF is quite different as the sway interaction IRF oscillate over time in Fig. 2(b) whilst the oscillations of IRF in Fig. 2(a) decay to zero after just nondimensional time of 4.

The diagonal sway added-mass and damping coefficients of ITU-WAVE are presented in Fig. 3(a) and (3b) respectively with analytical results of [18] for comparison purposes. The comparison of present numerical results with analytical results shows satisfactory agreements. The added mass $A^{11}_{22}(\omega)$ and damping coefficients $B^{11}_{22}(\omega)$ in Fig. 3(a) and (b) in the present paper are obtained by Fourier transform of time dependent sway IRF in Fig. 2(a) as the frequency and time domain results depend on each other through Fourier transform.

The sway interaction added mass $A^{13}_{22}(\omega)$ and damping coefficients $B^{13}_{22}(\omega)$ between WEC1 and WEC3 of present ITU-WAVE results and analytical results [18], which show satisfactory agreements, are presented in Fig. 4(a) and (b) respectively. Added mass and damping coefficients in Fig. 4(a) and (b) are obtained by Fourier transform of sway IRF, $K^{13}_{22}(t)$, of Fig. 2(b).

4.1.2. Validation of exciting force amplitudes

The heave exciting IRFs of linear 1 × 5 arrays of truncated vertical cylinder with separation distance between WECs d = 4R as well as between a vertical wall and WECs wl = 4R, and draft T = 2R at heading angle $\beta = 90°$ is presented in Fig. 5(a). The heave exciting IRFs are the same for K^1_{3E} and K^5_{3E} as well as K^2_{3E} and K^4_{3E} due to symmetry of WECs with respect to heading angle 90°. In K^1_{3E}, subscript represents the mode of motion (e.g., 3E for heave mode whilst E is for exciting force) whilst the superscript is used for WEC number (e.g., 1 is for the first WEC in an array system in Fig. 1). The exciting IRFs in sway mode K^1_{2E} of linear 1 × 5 arrays of truncated vertical cylinder with draft R, separation distance between WECs 8R as well as between a vertical wall and WECs 4R at heading angle 90° are presented in Fig. 5(b). Fig. 5(b) also shows Froude-Krylov IRF (K^1_{2FK}), diffraction IRF (K^1_{2D}), and exciting force IRF (K^1_{2E}) which is the superposition of Froude-Krylov and diffraction IRFs. K^1_{2FK} is predicted in the absence of WECs whilst K^1_{2D} represents the effect of diffracted waves from each WEC in an array system. K^1_{2D} is the functions of the size of WECs geometries with respect to incident wavelength.

The heave exciting force amplitudes for F^1_{3E} and F^5_{3E}, F^2_{3E} and F^4_{3E}, F^3_{3E} of linear 1 × 5 arrays are presented in Fig. 6(a), (b) and (c) respectively together with numerical results of [41]. It can be observed in Fig. 6 that comparison of numerical results shows satisfactory agreements. The exciting force amplitudes in Fig. 6(a), (b), and (c) are obtained by Fourier transform of the exciting force IRFs of Fig. 5(a). The present numerical results without a vertical wall are also presented to show the effects of a vertical wall. When the numerical results with and without vertical wall effects are compared, it can be observed from Fig. 6(a), (b), and (c) that the amplitudes of heave exciting force in front of a vertical wall are almost two times greater than those of heave exciting force

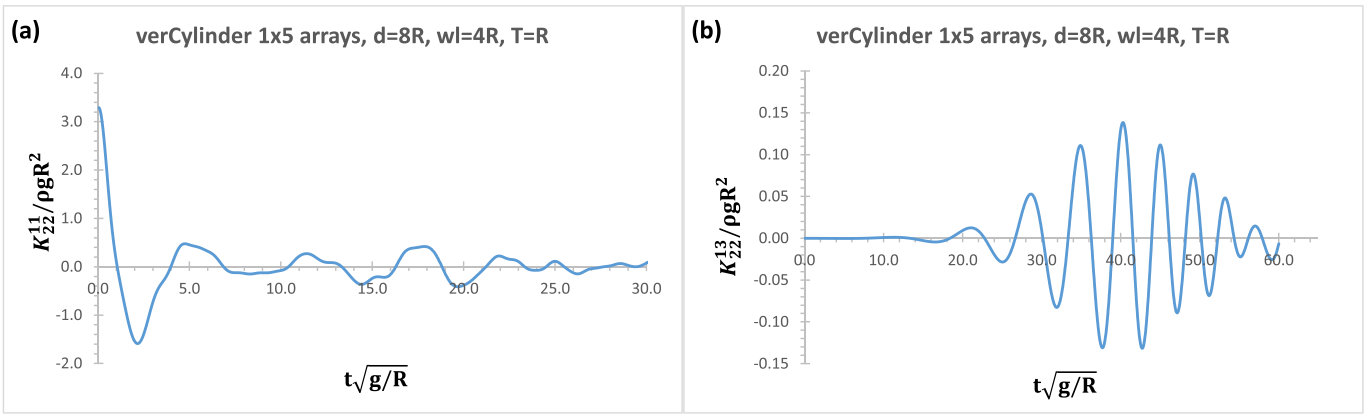

Fig. 2. Nondimensional sway radiation IRFs of WEC1 in linear 1 × 5 arrays of truncated vertical cylinder in front of a vertical wall (a) diagonal $\boldsymbol{K}_{22}^{11}(\boldsymbol{t})$ IRF (b) interaction $\boldsymbol{K}_{22}^{13}(\boldsymbol{t})$ IRF.

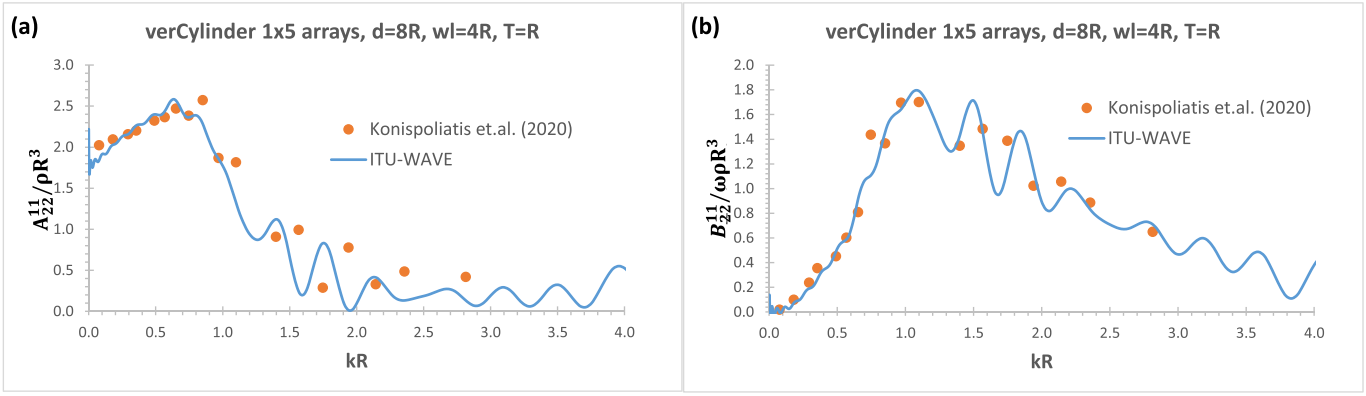

Fig. 3. Nondimensional diagonal sway coefficients of WEC1 (a) added mass, $\boldsymbol{A}_{22}^{11}(\boldsymbol{\omega})$ (b) damping, $\boldsymbol{B}_{22}^{11}(\boldsymbol{\omega})$.

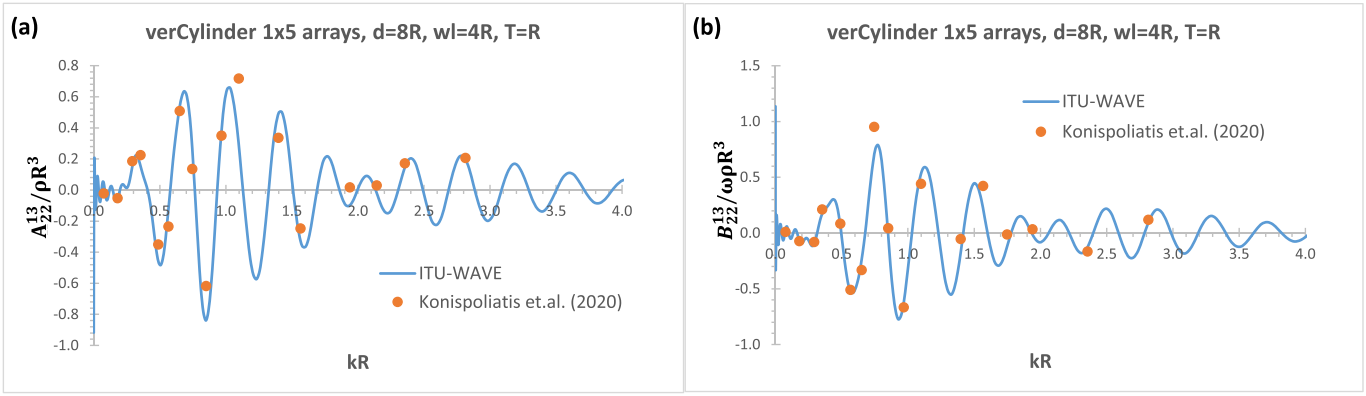

Fig. 4. Nondimensional interaction sway coefficients between WEC1 and WEC3 (a) added mass, $\boldsymbol{A}_{22}^{13}(\boldsymbol{\omega})$ (b) damping, $\boldsymbol{B}_{22}^{13}(\boldsymbol{\omega})$.

amplitude without a wall effect at zero frequency whilst the behaviour of the exciting force amplitudes at the intermediate frequencies shows significantly different behaviour especially in sway mode in Fig. 6(d). The sway exciting force amplitude of F_{2E}^{1} for linear 1 × 5 arrays of truncated vertical cylinder is presented in Fig. 6(d) together with analytical results of [18] which are in satisfactory agreements.

4.1.3. Validation of response amplitude operators (RAOs)

Heave RAOs of the present ITU-WAVE numerical results for sphere with linear 1 × 5 arrays and without vertical wall effects are presented and compared with experimental results [42] in Fig. 7.

The separation distance between WECs and heading angle are 4R and 90° respectively. Heave RAOs of x_3^1 and x_3^5 as well as x_3^2 and x_3^4 are the same due to symmetry of WECs with respect to heading angle 90° although the experimental results do not show the symmetric behaviour and do not satisfy the symmetry condition with respect to incoming incident wave 90°. In x_3^5, subscript is for mode of motion (e.g., 3 represents heave mode) whilst superscript is for WEC number in the array (e.g., 5 represents 5th WEC in the array system). One of the reasons of unsymmetrical behaviour of

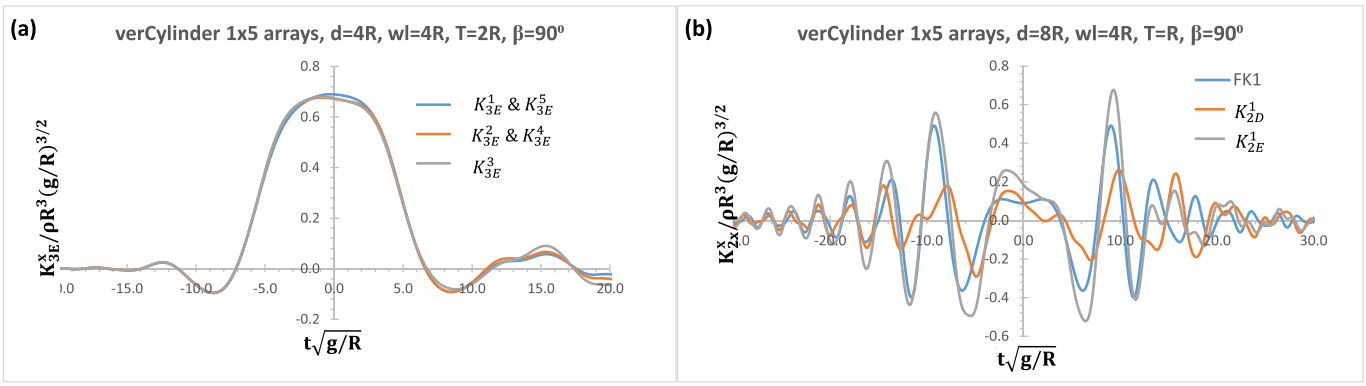

Fig. 5. Nondimensional IRFs (a) heave IRFs, K^1_{3E}- K^5_{3E} (b) sway IRFs, K^1_{2FK}, K^1_{2D}, K^1_{2E}.

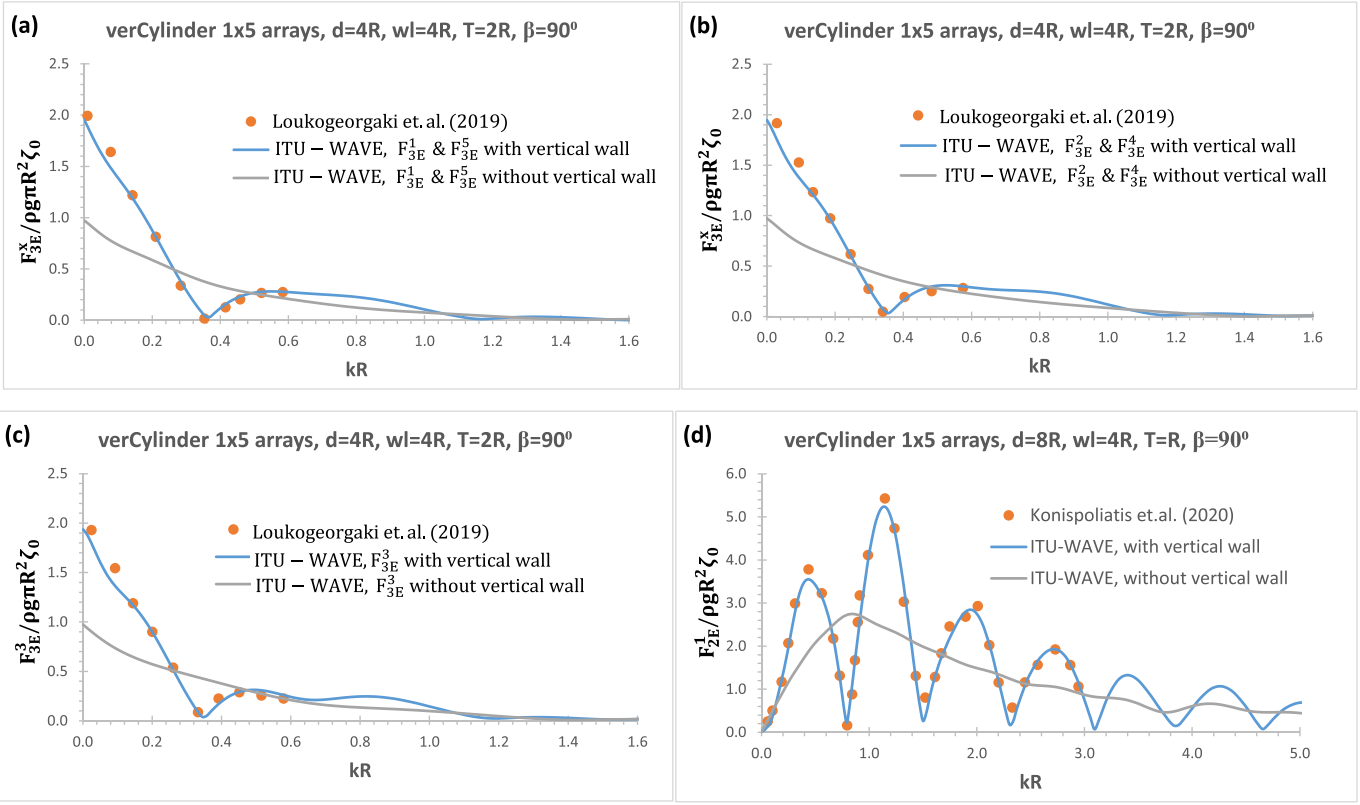

Fig. 6. Nondimensional exciting force amplitudes (a) F^1_{3E} and F^5_{3E} (b) F^2_{3E} and F^4_{3E} (c) F^3_{3E} (d) F^1_{2E}.

the experimental work could be due to the way that the experimental investigation is set up. The present ITU-WAVE numerical and experimental results [42] show satisfactory agreement in Fig. 7.

4.2. RAOs of linear 1 × 5 arrays of truncated vertical cylinders

Heave RAO for linear 1 × 5 arrays of truncated vertical cylinder with separation distance between WECs 4R, draft 2R and in a range of separation distances between a vertical wall and WECs at heading angle 90° are presented in Fig. 8. Heave RAOs without a vertical wall effect is also presented for comparison purposes. The greater heave motion amplitudes implicitly mean that more wave power would be captured in an array system.

As there are no velocity and acceleration at lower incident wave frequencies, the heave motion is controlled by restoring forces and WECs in an array system have immediate response to the incident waves when they disturb at their mean positions. As the mass of WECs are balanced with restoring forces at and around heave natural frequency ($\omega_n = 2$ rad/s) region, the heave motion at this resonance region is controlled by wave damping. In the case of higher frequencies, the heave motion is controlled by the mass of WECs. As WECs in an array system would not have enough time to response, the motion decays to zero at higher frequencies. The heave motion amplitude in Fig. 8 is greater in the case of closer separation distance between a vertical wall and WECs (e.g., 1.5R) whilst keeping separation distance between WECs constant (e.g., 4R). This is due to nearly trapped waves in the gap and standing waves between WECs as well as between WECs and a vertical wall. It is also due to the stronger hydrodynamic interactions at closer proximity. When the heave amplitudes of WECs are considered in

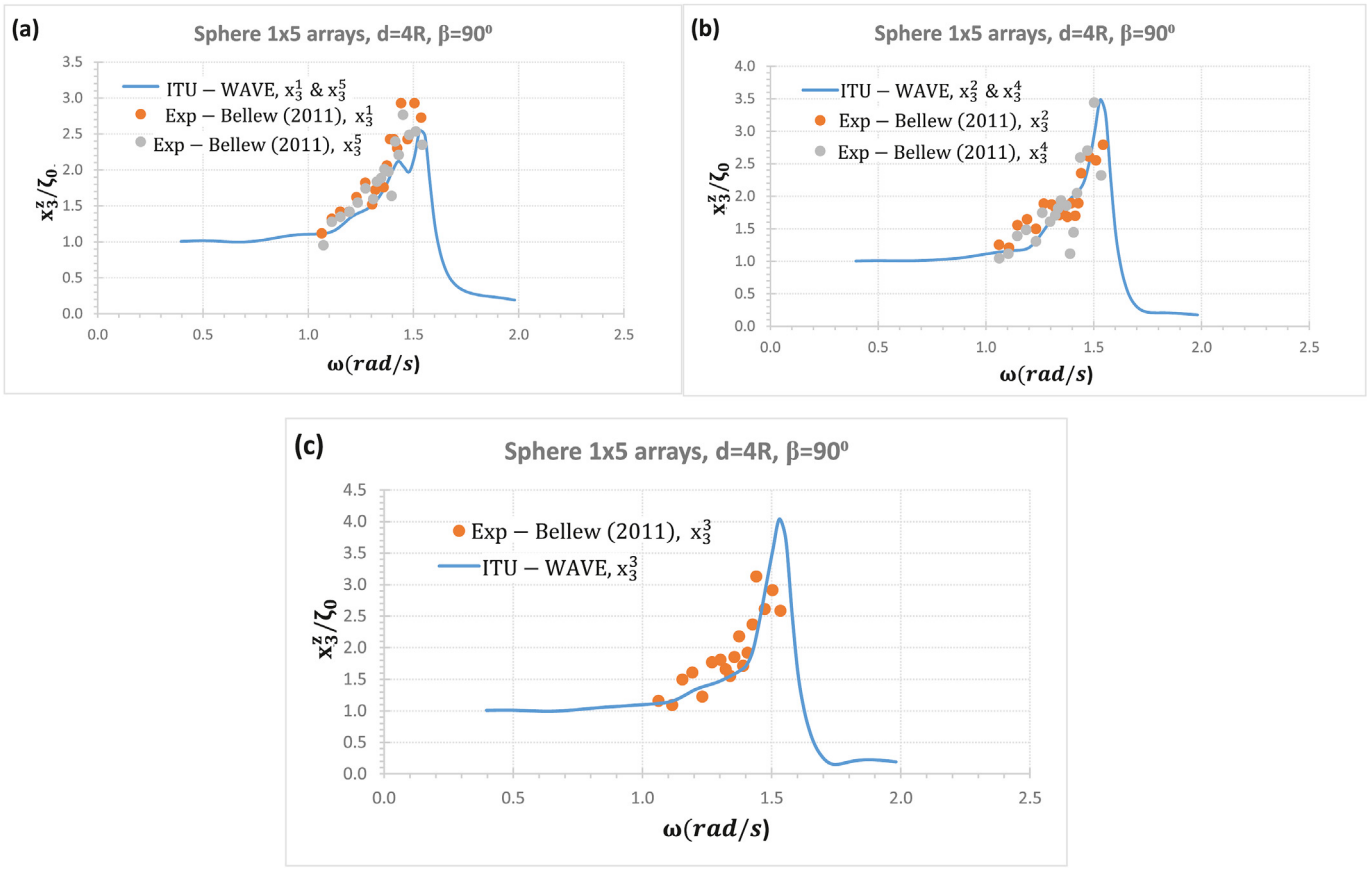

Fig. 7. Nondimensional heave RAOs (a) $\boldsymbol{x}_3^1$ and $\boldsymbol{x}_3^5$ (b) $\boldsymbol{x}_3^2$ and $\boldsymbol{x}_3^4$ (c) $\boldsymbol{x}_3^3$.

Fig. 8(a) and (b) and 8(c), WEC3 (which is in the middle of linear 1×5 array system) experiences the greatest amplitude at the heave resonance region compared to other WECs due to stronger hydrodynamic interaction, standing waves and nearly trapped waves in the gap of the array system around WEC3.

4.3. Wave power absorption from ocean waves

The wave power absorption from ocean waves as a function of incident wave frequencies in a range of separation distance between a vertical wall and WECs at heading angle 90° is presented in Fig. 9. The maximum wave power is absorbed with separation distance between a vertical wall and WECs of 1.5R as the strongest hydrodynamic interaction occurs at closer separations distances. It is theoretically known [33] that the maximum wave power is absorbed at and around resonant frequency ($\omega_n = 2$ rad/s) as it is also observed in Fig. 9.

The absorbed wave power decreases due to the weaker hydrodynamic interaction in Fig. 9 when the separation distance between a vertical wall and WECs increases (e.g., $wl = 3.5$R). Less wave power is absorbed with a vertical wall effect compared to without a vertical wall when the separation distance between a vertical wall and WECs is greater than $wl = 2$R. This is due to weaker hydrodynamic interactions between gaps of WECs as well as WECs and a vertical wall.

4.4. Effects of separation distances on mean interaction factor ($\boldsymbol{q}_{\boldsymbol{mean}_k}$)

4.4.1. Variable separation distance between WECs keeping it constant between WECs and a vertical wall

The mean interaction factor q_{mean_k} with respect to a range of the incident wave frequencies, ω, with and without a vertical wall effect are presented in Fig. 10 at heading angle 90°. In q_{mean_k}, k represents mode of motion (e.g., $k = 3$ is for heave mode). A range of the separation distances between WECs are considered whilst the separation distance between a vertical wall and WECs are kept constant. The interactions between WECs in an array system are measured with mean interaction factor, $q_{mean_k}(\omega)$, for the interacting systems of N numbers of WECs. Mean interaction factor plays sensitive and significant role about the overall wave power absorption. Mean interaction factor can have constructive ($q_{mean_k}(\omega) > 1$) or destructive ($q_{mean_k}(\omega) < 1$) effect. The constructive effect implicitly means that wave power absorption from an array system increases in that wave frequency compared to wave power that is absorbed by an isolated N numbers of WECs whilst wave power absorption decreases in the case of destructive effect. The constructive effect with a vertical wall up to around the heave natural frequency ($\omega_n = 2$ rad/s) in Fig. 10 is approximately four times greater compared to mean interaction factors without vertical wall effect. However, in the case of vertical wall effect, in some separation distances between WECs (e.g., $d = 2.5$R and $wl = 1.5$R),

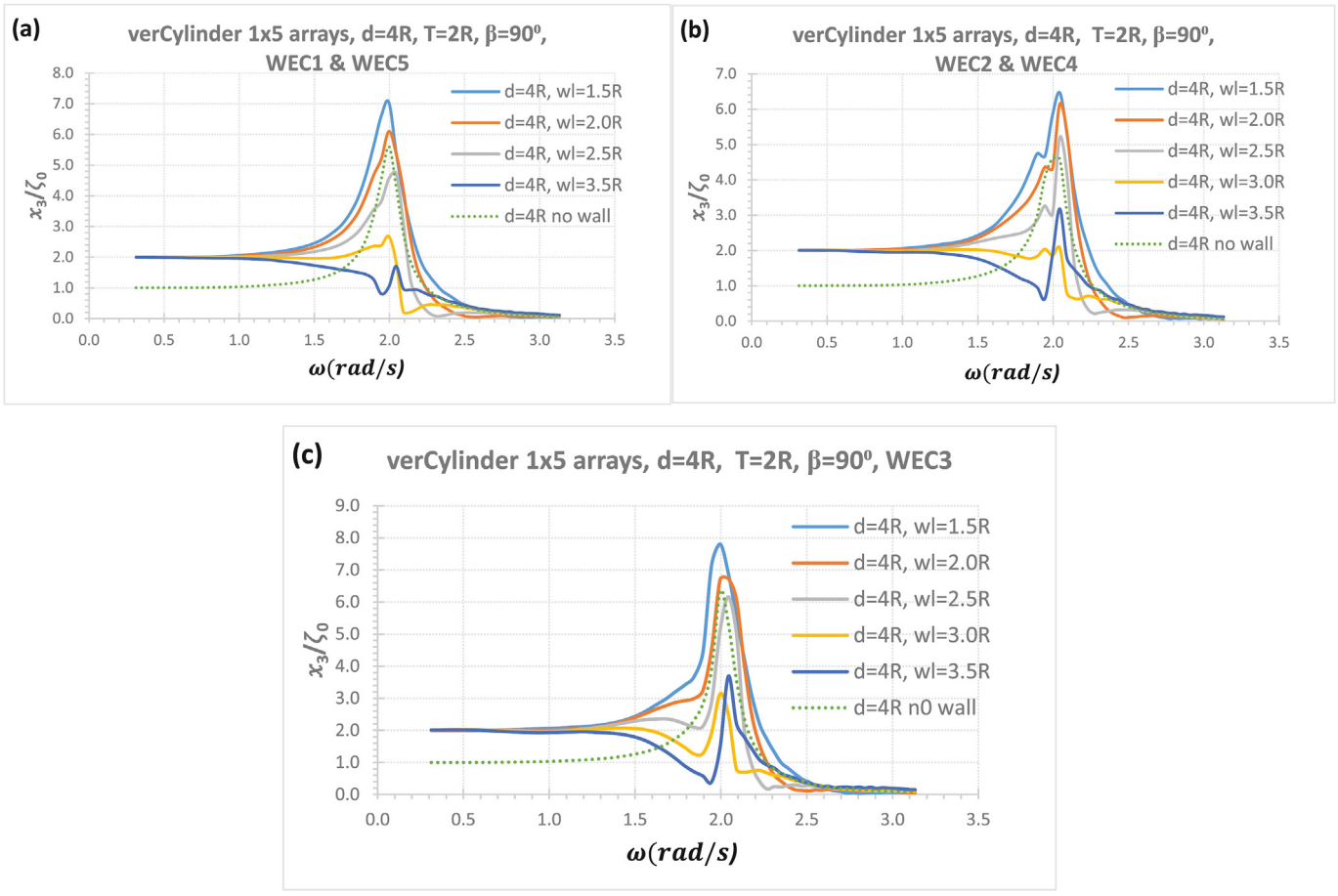

Fig. 8. Nondimensional heave RAOs (a) x_3^1 and x_3^5 (b) x_3^2 and x_3^4 (c) x_3^3.

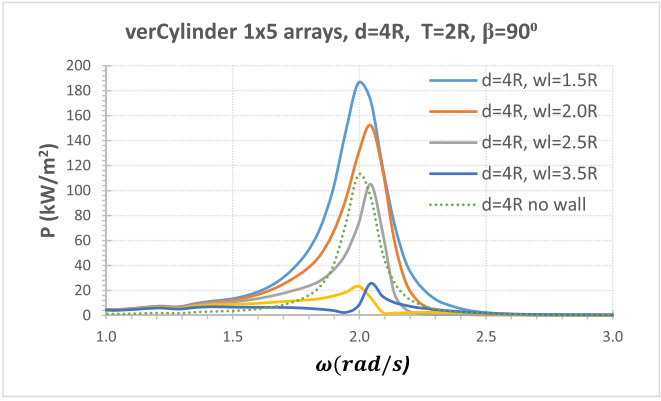

Fig. 9. Absorbed wave power in a range of incident wave frequency.

the constructive effect decreases just below one which is the limit for constructive effect. The constructive effect starts to recover again just after the heave natural frequency although the mean interaction factor shows destructive effect between 2.5 and 3.0 rad/s and then recover to constructive effect again.

In the case of without vertical wall effect, mean interaction factors q_{mean_3} equal to one up to around heave natural frequency ($\omega_n = 2$ rad/s). This implicitly means that there are no constructive and destructive effects as the same amount of wave power is absorbed with an array system and the same number of isolated WECs. As in a vertical wall effect, there are destructive effect in a range of separation distance at and around natural frequency whilst the constructive effects are recovered after the heave natural frequency. When the overall performance of linear 1 × 5 arrays with and without vertical wall effects are compared, it can be observed from Fig. 10 that arrays with a vertical wall perform much better than those of without a vertical wall.

4.4.2. *Variable separation distance between WECs and a vertical wall keeping it constant between WECs*

Mean interaction factor q_{mean_k} in a range of separation distances between a vertical wall and WECs are presented in Fig. 11. The constructive effect with a vertical wall effect in Fig. 11 is four times greater than that of without vertical wall effect at lower incident wave frequencies. However, this constructive effect decreases and approaches to zero between 1.5 rad/s and 2.0 rad/s incident wave frequencies.

Mean interaction factor shows the lowest destructive effect around heave natural frequency ($\omega_n = 2$ rad/s) with increasing separation distance between a vertical wall and WECs whilst keeping the separation distance between WECs constant (d =4R). The mean interaction factors start to recover the constructive effect just after around heave natural frequency for higher incident wave frequencies. When the mean interaction factors with and without vertical wall effects are compared, it can be observed from Fig. 11 that the performances of linear 1 × 5 arrays with a vertical wall effect demonstrate much better performances than those of

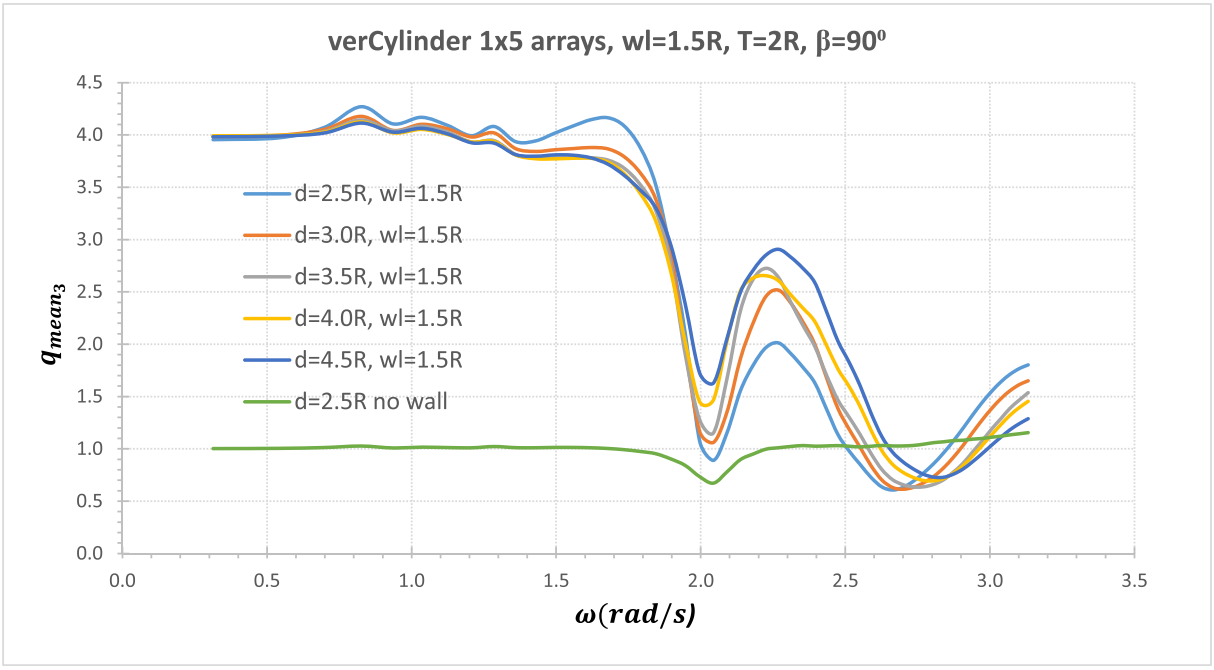

Fig. 10. Mean interaction factor of linear 1 × 5 arrays of truncated vertical cylinder in a range of separation distance between WECs at heading angle 90° with and without vertical wall effects.

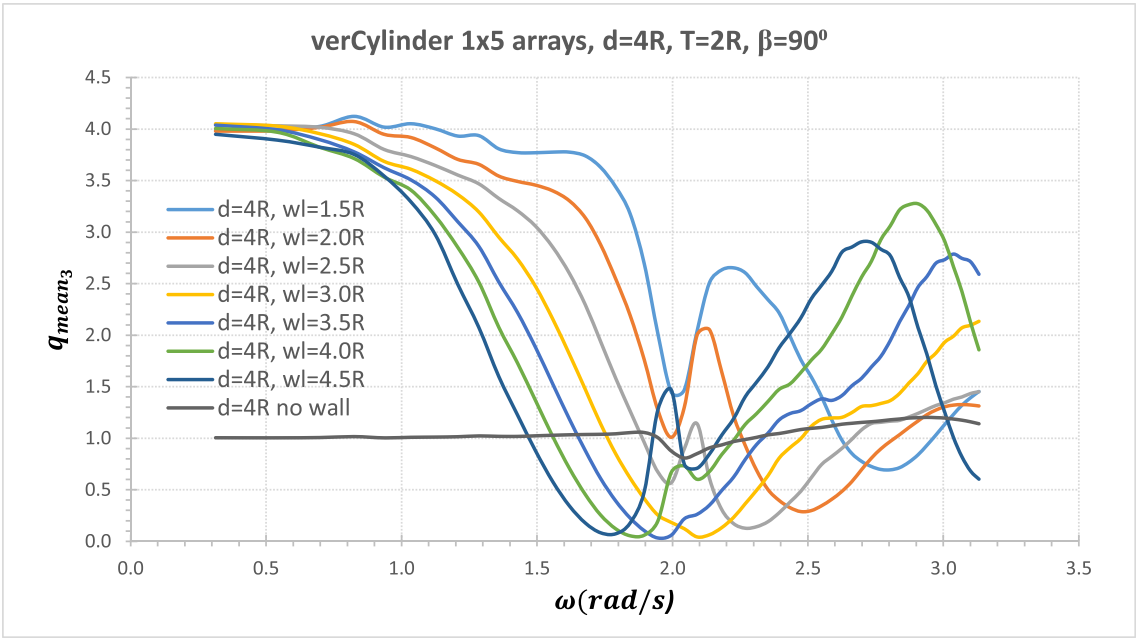

Fig. 11. Mean interaction factor of linear 1 × 5 arrays of truncated vertical cylinder in front of vertical wall at heading angle 90°.

without a vertical wall in all separation distances of a vertical wall and WECs.

4.5. Effects of heading angles on mean interaction factor (q_{mean_k})

4.5.1. Constant separation distance between WECs and without a vertical wall effect

Mean interaction factors q_{mean_3} without a vertical wall effect for different heading angles are presented in Fig. 12. It can be observed in Fig. 12 that up to the incident wave frequency of 1.5 rad/s, the constructive and destructive effects in a range of heading angles are more or else the same. However, the substantive differences occur around and after the heave natural frequency ($\omega_n = 2$ rad/s).

As shown in Fig. 1, heading angle is represented with 180° being the incident wave parallel to 1 × 5 arrays of truncated vertical cylinder whilst the beam seas are represented with 90° being the incident wave perpendicular to linear 1 × 5 arrays. When the incident wave angles of 180° and 150° are observed it may be noticed that mean interaction factor shows the constructive effects just before the heave natural frequency ($\omega_n = 2$ rad/s). However,

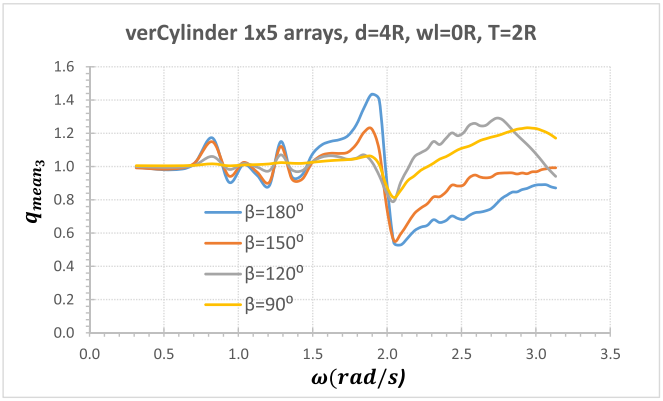

Fig. 12. Mean interaction factor of linear 1 × 5 arrays of truncated vertical cylinder without vertical wall effect in a range of heading angles.

after heave natural frequency, the hydrodynamic interactions between WECs shows destructive effects which continue over higher incident wave frequencies. In the case of the heading angles 120° and 90°, there are no constructive or destructive effects up to heave natural frequency which means the absorbed wave power with linear 1 × 5 arrays, and five isolated truncated vertical cylinders is the same. However, just after heave natural frequency, hydrodynamic interaction first shows destructive effect, and the wave interaction then demonstrates the trend of constructive effects over high incident wave frequencies. When the mean interaction factor of heading angles of 90° and 120° are compared, just after heave natural frequency, heading angle 120° shows better constructive effect whilst it is 90° which demonstrates better constructive effects at higher incident wave frequencies.

4.5.2. Constant separation distance between WECs as well as WECs and a vertical wall

The mean interaction factors q_{mean_3} with a vertical wall effect for different heading angles are presented in Fig. 13. When the performance of linear 1 × 5 arrays without and with vertical wall effects is compared for different heading angles in Figs. 12 and 13 respectively, the performance of WECs with a vertical wall effect is much greater than that of without a vertical wall effect in a range of wave frequencies and heading angles.

When the performance of linear 1 × 5 array system is compared with respect to heading angles in Fig. 13, the most dominant heading angle in heave mode is 180°. Mean interaction factors in

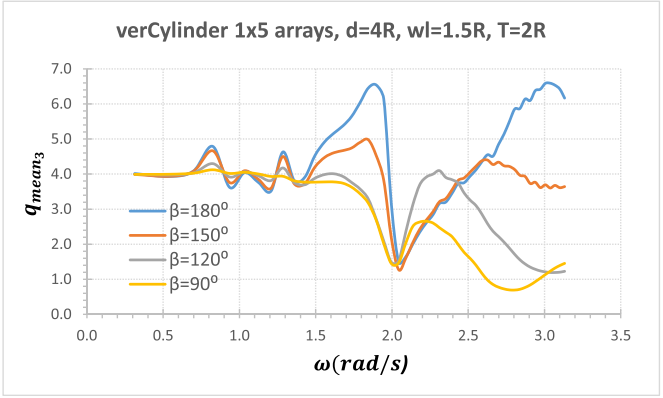

Fig. 13. Mean interaction factor of linear 1 × 5 arrays of truncated vertical cylinder with a vertical wall effect in a range of heading angles.

Fig. 13 show much better constructive effects compared to linear 1 × 5 arrays without a vertical wall effect in Fig. 12 up to heave natural frequency and then demonstrate sudden decreases at natural frequency. However, this decrement effects are recovered at higher incident wave frequencies at heading angles 180° and 150°. In the case of heading angles 120° and 90°, the performance of linear 1 × 5 array system shows the steady constructive effect although around natural frequency this effect demonstrates sudden decrease and then shows recovery at higher incident wave frequencies and drops again.

4.6. Effects of heading angles on individual interaction factor ($q^i_{indv_k}$)

4.6.1. Constant separation distance between WECs and without a vertical wall effect

Individual interaction factors $q^i_{indv_3}$ with respect to incident wave frequencies, ω, for linear 1 × 5 arrays of truncated vertical cylinder without a vertical wall effect are presented in Fig. 14(a) and (b), 14(c) and 14(d) for heading angles of 180°, 150°, 120° and 90° respectively. In $q^i_{indv_k}$, k represents mode of motions (e.g., 3 is used for heave mode) whilst i is used for the positions of WCs in an array system (e.g., $i = 2$ is used WEC2).

WEC1 ($q^1_{indv_3}$) has constructive effect for 180°, 150° and 120°. In the case of 90°, $q^1_{indv_3}$ also has constructive effect up to heave natural frequency ($\omega_n = 2$ rad/s), however, just after the natural frequency WEC1 has destructive effect. WEC2 ($q^2_{indv_3}$) shows constructive effect up to heave natural frequency and just after natural frequency it has destructive effect for heading angles 180° and 150°. $q^2_{indv_3}$ shows much better performance over a range of the incident wave frequency with constructive effect at 120° and 90°. WEC3 ($q^3_{indv_3}$), which is in the middle of the array system, shows destructive characteristics in a range of the incident wave frequencies at the heading angle 180°. In addition, $q^3_{indv_3}$ shows destructive effect up to heave natural frequency and then shows constructive effects after it at the heading angles 150° and 120°. At heading angle 90°, WEC3 has constructive effect over a range of the incident wave frequencies. $q^4_{indv_3}$ and $q^5_{indv_3}$ show constructive effect up to heave natural frequency and destructive effect after it at heading angle 180° and 150°. $q^4_{indv_3}$ shows destructive effect in a range of incident wave frequencies at heading angle 120° whilst $q^5_{indv_3}$ has destructive effect up to heave natural frequency and then constructive effect after it. $q^4_{indv_3}$ shows constructive effects over incident wave frequencies whilst $q^5_{indv_3}$ has destructive effect at heading angle 90°.

4.6.2. Constant separation distance between WECs as well as WEC and a vertical wall

The performance of each $q^i_{indv_3}$ in an array system is measured by individual interaction factor $q^i_{indv_k}$ which is presented in Fig. 15(a) and (b), 15(c), 15(d) and 15(e) as the function of heading angles.

When the performances of $q^i_{indv_3}$ without and with vertical wall effects are compared in Figs. 14 and 15 respectively, the performance of WECs arrays with a vertical wall are approximately four times greater than those of $q^i_{indv_3}$ without a vertical wall at lower frequencies whilst the performance of WECs arrays at higher frequencies are even better. The hydrodynamic interactions in the gap of WECs arrays as well as a vertical wall and WECs arrays contribute

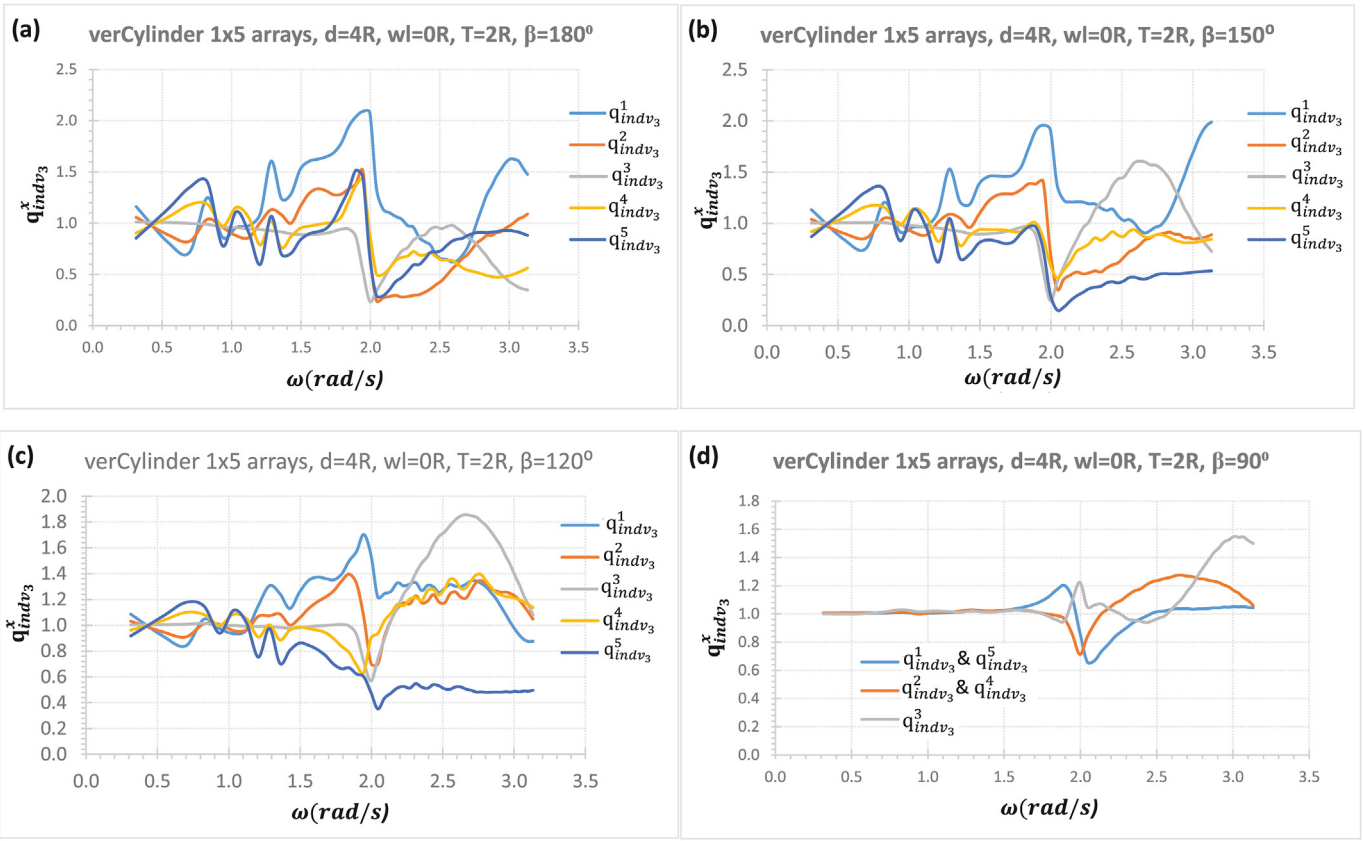

Fig. 14. Individual interaction factor of linear 1 × 5 arrays of truncated vertical cylinder without vertical wall effect in a range of heading angles (a) 180° (b) 150° (c) 120° (d) 90°.

to the constructive effect for all WECs in linear 1 × 5 arrays of truncated vertical cylinder. It can be observed from Fig. 15(a) and (b) that the best performances are observed for $q^1_{ind_{v_3}}$, $q^2_{ind_{v_3}}$ and $q^4_{ind_{v_3}}$ at heading angles 180°, 150°, 120° and 90° respectively while it is the heading angles 150°, 180°, 120° and 90° for $q^3_{ind_{v_3}}$ which is in the middle of linear 1 × 5 array. The dominant heading angles to absorb wave power for $q^5_{ind_{v_3}}$ are 180°, 90°, 150° and 120° respectively. It may be noticed for $q^1_{ind_{v_3}}$ in Fig. 15(a) that the heading angle 180° shows dominant behaviour especially at higher incident wave frequencies. The interaction effect in Fig. 15(a) is getting weaker when the heading angle change from 180° to 90°.

5. Conclusions

The in-house ITU-WAVE transient free-surface three-dimensional wave-multibody interaction numerical tool is used to extend its application to wave power absorption from ocean waves in front of a vertical wall. The initial-value BIE is solved with time marching source formulation which takes a vertical wall effect into account with method of images exploiting perfect reflection of the incident waves.

Before ITU-WAVE computational tool is used for the prediction of wave power absorption in front of a vertical wall with WECs arrays, ITU-WAVE numerical results are validated against other numerical, analytical, and experimental results. These results include the added mass, damping coefficient, exciting force amplitude and RAOs in sway and heave modes. Sway and heave radiation and exciting force IRFs are first predicted with the solution of time dependent boundary integral equation. As the time and frequency domain results are linked to each other through Fourier transform in the context of linear analysis, the added mass, and damping coefficients as well as exciting force amplitudes are then obtained by taking Fourier transform of IRFs.

The sensitivity analysis of 1 × 5 array of truncated vertical cylinder with and without vertical wall effects is used to determine the effect of separation distance between WECs arrays as well as between a vertical wall and WECs arrays, and different heading angles on mean and individual interaction factors. The numerical experiences demonstrate that mean and individual interaction factors can have constructive or destructive effect in a range of incident wave frequencies.

The numerical experiences show that the performance of WECs in an array system in front of a vertical wall are much better than those of without a wall effect especially when the separation distance between a vertical wall and WECs arrays are at closer proximity. This is mainly due to nearly trapped waves and standing waves between WECs arrays as well as a vertical wall and WECs arrays. Mean and individual interaction factors are four times greater in the case of arrays in front of a vertical wall compared to without a vertical wall at lower frequencies although this constructive effect decreases to around one at the resonant frequency and then again increase showing constructive effect at higher frequencies.

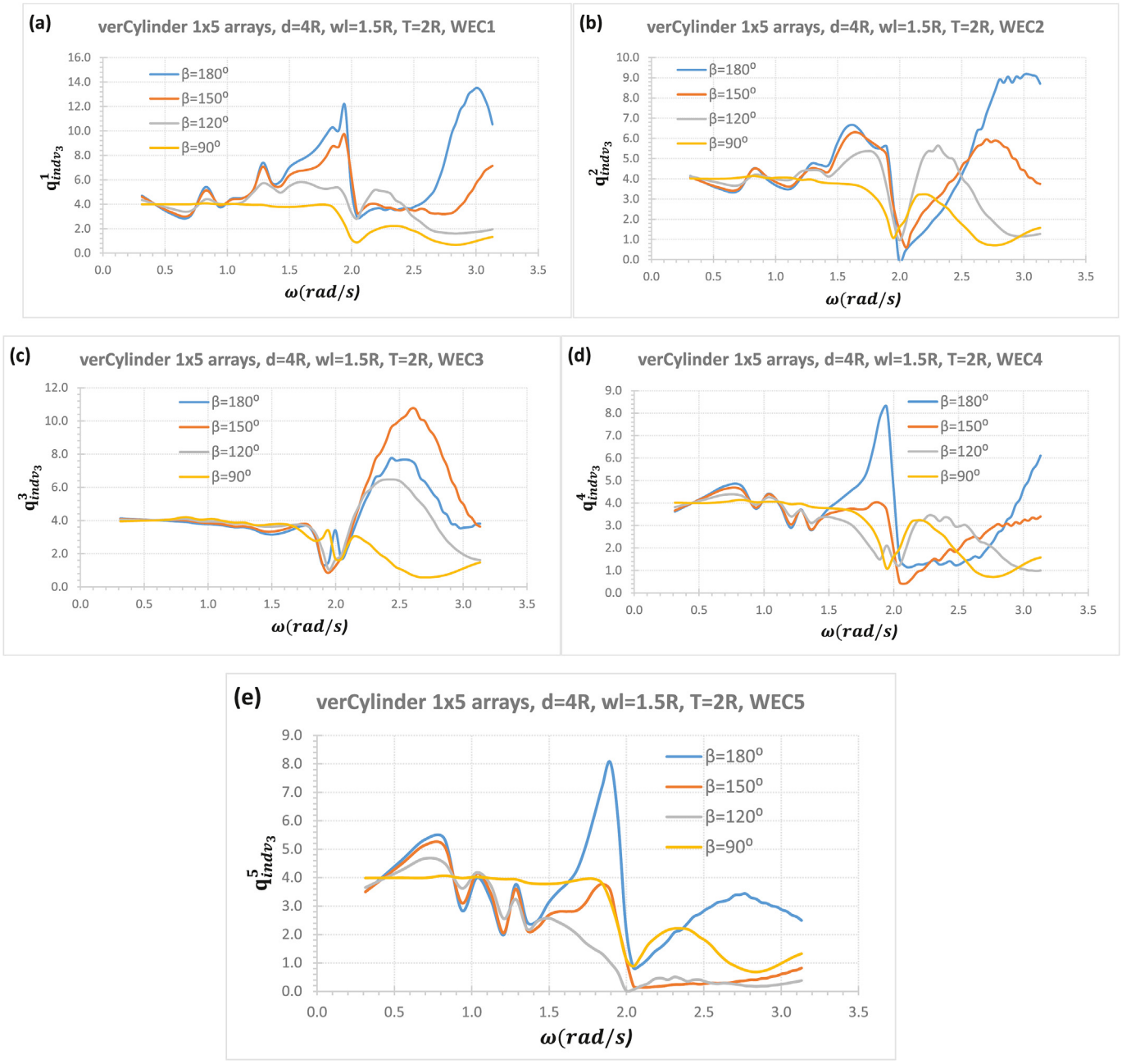

Fig. 15. Individual interaction factor of linear 1 × 5 arrays of truncated vertical cylinder in front of a vertical wall with separation (a) $q^1_{indv_3}$ (b) $q^2_{indv_3}$ (c) $q^3_{indv_3}$ (d) $q^4_{indv_3}$ (e) $q^5_{indv_3}$.

CRediT authorship contribution statement

Fuat Kara: Conceptualization, Methodology, Software, Validation, Formal analysis, Investigation, Resources, Data curation, Writing – original draft, Writing – review & editing, Visualization, Project administration.

Declaration of competing interest

The authors declare that they have no known competing financial interests or personal relationships that could have appeared to influence the work reported in this paper.

Acknowledgements

The present work is supported by Royal Academy of Engineering Newton Fund under the UK-China Industry Academy Partnership Programme (Grant No: UK-CIAPP\73). The author would like to acknowledge the financial support.

References

[1] F. Kara, Time domain prediction of power absorption from ocean waves with latching control, Renew. Energy 35 (2010) 423–434.
[2] F. Kara, Time domain prediction of power absorption from ocean waves with wave energy converters arrays, Renew. Energy 92 (2016) 30–46.
[3] M.A. Mustapa, O.B. Yaakob, Y.M. Ahmed, C.-K. Rheem, K.K. Koh, F.A. Adnan, Wave energy device and breakwater integration: a review, Renew. Sustain.

Energy Rev. 77 (2017) 43–58.
[4] X.L. Zhao, D.Z. Ning, Q.P. Zou, D.S. Qiao, S.Q. Cai, Hybrid floating breakwater-WEC system: a review, Ocean. Eng. 186 (2019) 106–126.
[5] F. Kara, Hydrodynamic performances of wave energy converters arrays in front of a vertical wall, Ocean. Eng. 235 (2021), 109459.
[6] E. Rusu, Evaluation of the wave energy conversion in various coastal environments, Energies 7 (2014) 4002–4018.
[7] R. Cascajo, E. Garcia, E. Quiles, A. Correcher, F. Morant, Integration of marine wave energy converters into seaports: a case study in port of Valencia, Energies 12 (2019) 787.
[8] J. Schay, J. Bhattacharjee, C.G. Soares, Numerical modelling of a heaving point absorber in front of a vertical wall, in: Proceedings of the ASME 32nd International Conference on Ocean, Offshore and Arctic Engineering, Nantes, France, 2013.
[9] C. Michailides, D.C. Angelides, Modeling of energy extraction and behavior of a flexible floating breakwater, Appl. Ocean Res. 35 (2012) 77–94.
[10] F. He, Z.H. Huang, A.W.K. Law, An experimental study of a floating breakwater with asymmetric pneumatic chambers for wave energy extraction, Appl. Energy 106 (2013) 222–231.
[11] S. Takahashi, Hydrodynamic characteristics of wave-power-extracting caisson breakwater, in: Twenty-First Coastal Engineering Conference, Costa del Sol, Malaga, Spain, 1988, pp. 2489–2503.
[12] P. Contestabile, E. Di Lauro, M. Buccino, D. Vicinanza, Economic assessment of overtopping breakwater for energy conversion (OBREC): a case study in western Australia, Sustainability 9 (2016) 51.
[13] C.Y. Yueh, S.H. Chuang, A boundary element model for a partially piston-type porous wave energy converter in gravity waves, Eng. Anal. Bound. Elem. 36 (2012) 658–664.
[14] D.Z. Ning, X.L. Zhao, M. Goteman, H.G. Kang, Hydrodynamic performance of a pile-restrained WEC-type floating breakwater: an experimental study, Renew. Energy 95 (2016) 531–541.
[15] J.N. Newman, in: Channel Wall Effects in Radiation-Diffraction Analysis, 31st International Workshop on Water Waves and Floating Bodies, 2016.
[16] E. Loukogeorgaki, I. Boufidi, I.K. Chatjigeorgiou, Performance of an array of oblate spheroidal heaving wave energy converters in front of a wall, Water 12 (2020) 188.
[17] X.L. Zhao, D.Z. Ning, D.F. Liang, Experimental investigation on hydrodynamic performance of a breakwater integrated WEC system, Ocean. Eng. 171 (2019) 25–32.
[18] D.N. Konispoliatis, S.A. Mavrakos, G.M. Katsaounis, Theoretical evaluation of the hydrodynamic characteristics of arrays of vertical axisymmetric floaters of arbitrary shape in front of a vertical breakwater, J. Mar. Sci. Eng. 8 (2020) 62.
[19] P. McIver, R. Porter, The motion of a freely floating cylinder in the presence of a wall and the approximation of resonances, J. Fluid Mech. 795 (2016) 581–610.
[20] S. Zheng, Y. Zhang, Wave radiation from a truncated cylinder in front of a vertical wall, Ocean. Eng. 111 (2016) 602–614.
[21] M.S. Chang, Computation of three-dimensional ship motions with forward speed, in: Proceedings of the 2nd International Symposium on Numerical Ship Hydrodynamics, University of California, Berkeley, 1977, pp. 124–135.
[22] F. Kara, Multibody interactions of floating bodies with time domain predictions, J. Waterw. Port, Coast. Ocean Eng. 146 (5) (2020).
[23] F. Kara, Time domain prediction of seakeeping behaviour of catamarans, Int. Shipbuild. Prog. 62 (3–4) (2016) 161–187.
[24] F. Kara, Applications of time domain methods for marine hydrodynamic and hydroelasticity analyses of floating systems, Ships Offshore Struct. (2021), https://doi.org/10.1080/17445302.2021.1937798.
[25] D. Nakos, D. Kring, P.D. Sclavounos, Rankine panel method for transient free surface flows, in: Proceedings of the 6th International Symposium on Numerical Hydrodynamics, Iowa City, I.A., USA, 1993, pp. 613–632.
[26] D.C. Kring, P.D. Sclavounos, Numerical stability analysis for time-domain ship motion simulations, J. Ship Res. 39 (4) (1995) 313–320.
[27] K. Budal, Theory for absorption of wave power by a system of interacting bodies, J. Ship Res. 21 (4) (1977) 248–253.
[28] M. Ohkusu, Wave action on groups of vertical circular cylinders, J. Soc. Nav. Archit. Jpn. 11 (1973) 37–50.
[29] H. Kagemoto, D.K.P. Yue, Interactions among multiple three-dimensional bodies in water waves: an exact algebraic method, J. Fluid Mech. 166 (1986) 189–209.
[30] W.E. Cummins, The Impulse response function and ship motions, Shiffstechnik 9 (1962) 101–109.
[31] T.F. Ogilvie, Recent progress toward the understanding and prediction of ship motions, in: Proceedings of the 5th Symposium on Naval Hydrodynamics, Office of Naval Research, Washington, D.C., USA, 1964, pp. 3–128.
[32] B.W. King, Time Domain Analysis of Wave Exciting Forces on Ships and Bodies, The University of Michigan, Ann Arbor, Michigan, USA, 1987. PhD thesis.
[33] K. Budal, J. Falnes, Optimum Operation of Wave Power Converter, Internal Report, Norwegian University of Science and Technology, 1976.
[34] F. Kara, Hydroelastic behaviour and analysis of marine structures, J. Sustain. Mar. Struct. 21 (1) (2021) 14–24.
[35] F. Kara, Time domain prediction of hydroelasticity of floating bodies, Appl. Ocean Res. 51 (2015) 1–13.
[36] F. Kara, Time domain potential and source methods and their application to twin-hull high speed crafts, Ships Offshore Struct. (2022), https://doi.org/10.1080/17445302.2022.2035560.
[37] J.L. Hess, A.M.O. Smith, Calculation of non-lifting potential flow about arbitrary three-dimensional bodies, J. Ship Res. 8 (1964) 22–44.
[38] S. Liapis, Time Domain Analysis of Ship Motions, The University of Michigan, Ann Arbor, Michigan, USA, 1986. PhD thesis.
[39] F. Kara, Time Domain Hydrodynamics and Hydroelastics Analysis of Floating Bodies with Forward Speed, University of Strathclyde, Glasgow, UK, 2000. PhD thesis.
[40] G.P. Thomas, D.V. Evans, Arrays of three-dimensional wave-energy absorbers, J. Fluid Mech. 108 (1981) 67–88.
[41] E. Loukogeorgaki, I.K. Chatjigeorgiou, Hydrodynamic performance of an array of truncated cylinders in front of a vertical wall, Ocean. Eng. 189 (2019), 106407.
[42] S. Bellew, Investigation of the Response of Groups of Wave Energy Devices, The University of Manchester, UK, 2011. PhD thesis.